

Ecological collapse and the emergence of traveling waves at the onset of shear turbulence

Hong-Yan Shih, Tsung-Lin Hsieh, Nigel Goldenfeld

Loomis Laboratory of Physics, University of Illinois at Urbana-Champaign, 1110 W. Green St., Urbana, IL 61801, USA

The transition to turbulence exhibits remarkable spatio-temporal behavior that continues to defy detailed understanding. Near the onset to turbulence in pipes, transient turbulent regions decay either directly or, at higher Reynolds numbers through splitting, with characteristic time-scales that exhibit a super-exponential dependence on Reynolds number. Here we report numerical simulations of transitional pipe flow, showing that a zonal flow emerges at large scales, activated by anisotropic turbulent fluctuations; in turn, the zonal flow suppresses the small-scale turbulence leading to stochastic predator-prey dynamics. We show that this “ecological” model of transitional turbulence reproduces the super-exponential lifetime statistics and phenomenology of pipe flow experiments. Our work demonstrates that a fluid on the edge of turbulence is mathematically analogous to an ecosystem on the edge of extinction, and provides an unbroken link between the equations of fluid dynamics and the directed percolation universality class.

Introduction. Fluids in motion are generally found in one of two generic states. The most common — turbulence — is found at sufficiently large characteristic speeds U , depending on the kinematic viscosity ν and the characteristic system scale D ; turbulent flows are complex, stochastic, and unpredictable in detail. At lower velocities, the fluid is said to be laminar: its flow is simple, deterministic and predictable. In between these two states, conventionally delineated by the dimensionless control parameter known as the Reynolds number $\text{Re} \equiv UD/\nu$, is a transitional regime that occurs for $1700 \lesssim \text{Re} \lesssim 2300$ in pipes, and which has presented a challenge to experiment and theory since Osborne Reynolds’ original observation of intermittent “flashes” of turbulence [1]. Today, Reynolds’ flashes are known as puffs [2], and their behavior has been characterized very precisely through a series of physical and numerical experiments performed during the last decade or so [3–6] (for a recent review, see [7]) culminating in the *tour de force* observation of a super-exponential functional dependence of the lifetime τ of puffs as a function of Re [8]: $\ln \ln \tau \propto \text{Re}$. For Reynolds numbers based upon pipe diameter D of around 2300, turbulence is sustained longer than the ability to observe its lifetime in finite systems, and the puffs become unstable through a new dynamical processes in which the leading edge breaks away and nucleates the formation of a new puff some distance downstream [9–12]. The puff-splitting occurs on a characteristic time that decays super-exponentially with increasing Re . Super-exponential scaling behavior near the transition to turbulence has also been reported in plane Couette flow [13] and Taylor-Couette flow [14].

The theoretical account of these phenomena has focused primarily on the existence and interactions between nonlinear solutions of the Navier-Stokes equations, particularly periodic orbits [15, 16], traveling waves [17–21] and the dynamics of long-lived chaotic transients [22]. An alternative line of inquiry has been to characterize the statistical properties of transitional turbulence through *ad hoc* model equations. These have been motivated ei-

ther by perceptive analogies to excitable media [23] or by phase transition universality arguments that begin with the notion that the laminar state is an absorbing one [24], and show quantitatively how super-exponential decay results from the generic universality class for non-equilibrium absorbing processes [25]: directed percolation (DP) [26]. Both approaches reflect an important aspect of the dynamics, namely that a certain minimum level of energy is required to sustain turbulent puffs [27], leading to a further connection with extreme value statistics [28].

It is the statistical behavior near the transition which concerns us here: how do the various spatial-temporal modes that are excited give rise to such remarkable lifetime statistics? What is the universality class of this transition, in terms of its fluctuation characteristics? Are there simplified effective descriptions that bridge the gap between the underlying fluid dynamics and the large-scale statistical properties? And how do these emerge from the underlying Navier-Stokes equations that govern all hydrodynamic phenomena?

Thus, we sought evidence for dynamical modes of the Navier-Stokes equations which exhibited an interplay between large-scale fluctuations and small-scale dynamics that would be captured by an effective statistical field theory description.

Observation of predator-prey dynamics in Navier-Stokes equations. To address these questions without making questionable or non-systematic approximations, we have performed direct numerical simulations (DNS) of the Navier-Stokes equations in a pipe, using the open-source code “Open Pipe Flow” [29], as described in Appendix A. We denote the time-dependent velocity deviation from the Hagen–Poiseuille flow by $\vec{u} = (u_z, u_\theta, u_r)$. Because we were interested in transitional behavior, we looked for large-scale modes that would indicate some form of collective behavior, as well as small-scale modes that would be representative of turbulent dynamics. In particular, we report here the behavior of the velocity field $(\bar{u}_z, \bar{u}_\theta, \bar{u}_r)$, where the bar denotes average over z

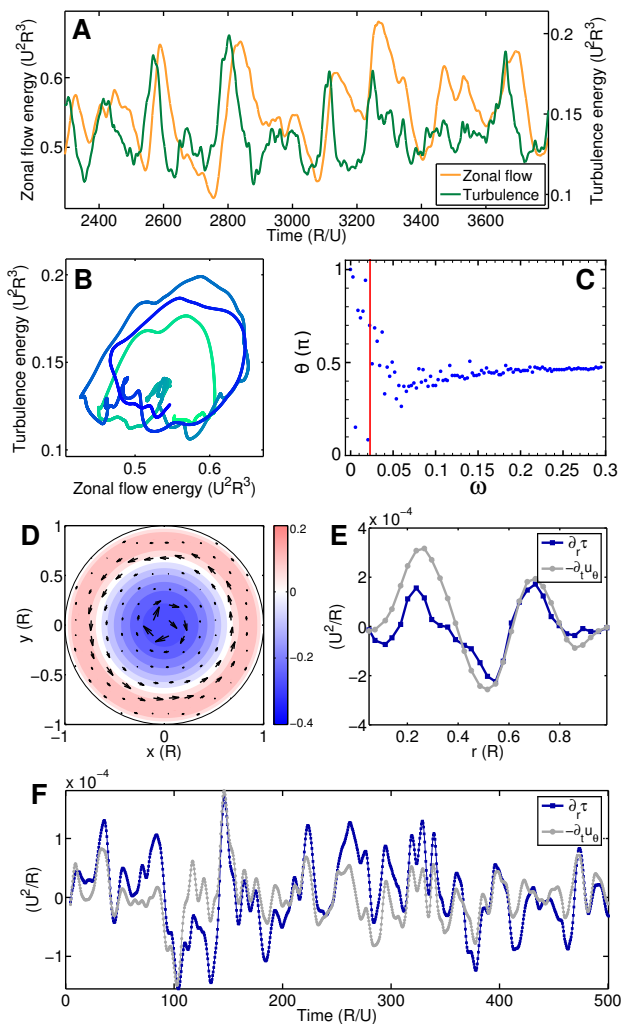


FIG. 1. Predator-prey oscillations in transitional turbulent pipe flow. (A) Energy vs. time for the zonal flow (orange) and turbulent modes (green). (B) Phase portrait of the zonal flow and turbulent modes as a function of time, with color indicating the earliest time in dark blue progressing to the latest time in light green. (C) Phase shift between the turbulent and zonal flow modes as a function of frequency, showing that the turbulence leads the zonal flow by $\pi/2$ consistent with predator-prey dynamics. The phase shift $\theta(\omega) = \tan^{-1} \left(\text{Im}[\tilde{C}(\omega)] / \text{Re}[\tilde{C}(\omega)] \right)$ and is shifted to be positive, where $\tilde{C}(\omega)$ is the Fourier transform of the correlation function between the turbulence and the zonal flow in (A). The red line corresponds to the dominant frequency in the power spectrum. The phase shift near small ω is scatter due to the finite time duration of the time series. (D) Velocity field configuration of the zonal flow mode \vec{u} . The color bar indicates the value of \bar{u}_z . (E) Snapshot of the Reynolds stress gradient and zonal flow time-derivative as functions of r . (F) Reynolds stress gradient and zonal flow time derivative as functions of time. The evident proportionality shows that zonal flow dynamics is driven by the radial gradient of the Reynolds stress.

and θ , and $\bar{u}_r = 0$. We refer to this as the zonal flow (ZF). In Fourier space, the zonal flow is given by $\tilde{u}(k=0, m=0, r)$, where k is the axial wavenumber and m is the azimuthal wavenumber, r is the real space radial coordinate and the tilde denotes Fourier transform in the θ and z directions only. Turbulence was represented by short-wavelength modes, whose energy is $E_T(t) \equiv \frac{1}{2} \sum_{|k| \geq 1, |m| \geq 1} \int |\tilde{u}(k, m, r)|^2 dV$.

Shown in Figure 1(A) is a time series for the energy $E_{ZF}(t)$ of the zonal flow, compared with the energy $E_T(t)$ of the turbulent energy. The curves show clear persistent oscillatory behavior, modulated by long-wavelength stochasticity as shown in the phase portrait of Figure 1(B). In Figure 1(C), we have calculated the phase shift between the turbulence and zonal flows, with the result that the turbulent energy leads the zonal flow energy by $\sim \pi/2$. This suggests that these oscillations can be interpreted as a time-series resulting from activator-inhibitor dynamics, such as occurs in a predator-prey ecosystem. Predator-prey ecosystems are characterized by the following behavior: the ‘‘prey’’ mode activates the ‘‘predator’’ mode, which then grows in abundance. At the same time, the growing predator mode begins to inhibit the prey mode. The inhibition of the prey mode starves the predator mode, and it too becomes inhibited. The inhibition of the predator mode allows the prey mode to re-activate, and the population cycle begins again.

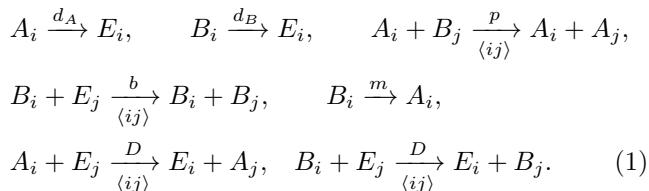
The flow configuration for the predator mode is shown in Figure 1 (D), and consists of a series of azimuthally symmetric modes with direction reversals as a function of radius r . Such banded shear flows are known as zonal flows and are of special significance in plasma physics, astrophysical and geophysical flows, owing to their role in regulating turbulence [30]. The purely azimuthal component of the zonal flow, denoted by $\bar{u}_\theta(r)$ is spatially uniform in z , and the lack of a radial component means that it is not driven by pressure gradients. Thus it can only exist due to nonlinear interactions with turbulent modes. In this sense, it is a collective mode, one with special significance for transitional turbulence.

The simplest way for such an azimuthal shear flow to couple to turbulent fluctuations is through the Reynolds stress τ : however, a uniform Reynolds stress cannot drive a shear flow, so the first symmetry-allowed possibility is the radial gradient of the Reynolds stress [30], as expressed in the Reynolds momentum equation. Thus, to probe the dynamics that govern the emergence of the zonal flow, we have calculated the time-averaged radial gradient of the instantaneous Reynolds stress, $\tau \equiv u'_\theta \cdot u'_r$, where $\vec{u}'(z, \theta, r) \equiv \vec{u} - \bar{\vec{u}}$, and show in Figure 1 (F) the 4.5-time-unit-running-mean time series of $-\partial_t \bar{u}_\theta$ and the radial gradient $\partial_r \tau$. Both quantities have been averaged over $0 \leq z \leq L$, $0 \leq \theta \leq 2\pi$ and $R_0 \leq r < R$, where $R_0 = 0.641R$, and the resulting time series are clearly highly correlated.

In general, it is the case that zonal flows are driven by statistical anisotropy in turbulence, but are themselves an isotropizing influence on the turbulence through their

coupling to the Reynolds stress [31–33]. The fact that turbulence anisotropy activates the zonal flow, and that zonal flow inhibits the turbulence is responsible for the predator-prey oscillations observed in the numerical simulations.

Lifetime of stochastic predator-prey populations. Phase transition theory [34] would suggest that the emergence of a zonal flow collective mode dominates the non-equilibrium transition of pipe flow from the laminar to the turbulent state, through the predator-prey interaction with the small scale velocity fluctuations. Such a “two fluid” effective field description of transitional turbulence implies that stochastic predator-prey populations should undergo spatio-temporal fluctuations whose functional form matches precisely the observations for the lifetime and splitting time of turbulent puffs in a pipe. To test this idea, we have performed simulations of a spatially-extended stochastic predator-prey ecosystem, in a quasi-one-dimensional geometry to mimic the pipe environment. The specific system has three trophic levels: nutrient (E), Prey (B) and Predator (A), which correspond in the fluid system to laminar flow, turbulence and zonal flow respectively. The interactions between individual representatives of these levels are given by the following rate equations



where d_A and d_B are the death rates of A and B, p is the predation rate, b is the prey birth rate due to consumption of nutrient, $\langle ij \rangle$ denotes hopping to nearest neighbor sites, D is the nearest-neighbor hopping rate, and m is the point mutation rate from prey to predator, which models the induction of the zonal flow from the turbulence degrees of freedom.

We are primarily interested in long-wavelength properties of the system, at least in the vicinity of the turbulence transition, where we expect the transverse correlation length to be larger than the pipe diameter, implying that the behavior is in fact quasi-one-dimensional. The crossover phenomena associated with this have been discussed previously [26], and thus our quasi-one-dimensional model should be appropriate and quantitatively correct near the transition.

In our simulation, described in Appendix B, the control parameter is the prey birth rate b . When b is small enough, the population is metastable, and cannot sustain itself: all individuals, both predator and prey, eventually die within a finite lifetime $\tau(b)$. As b increases, the lifetime of the population increases rapidly: in particular the prey lifetime increases rapidly with b . At large enough values of b , the decay of the initial population is not observed, but instead the initially localized population proliferates, spreading outwards and spontaneously splitting

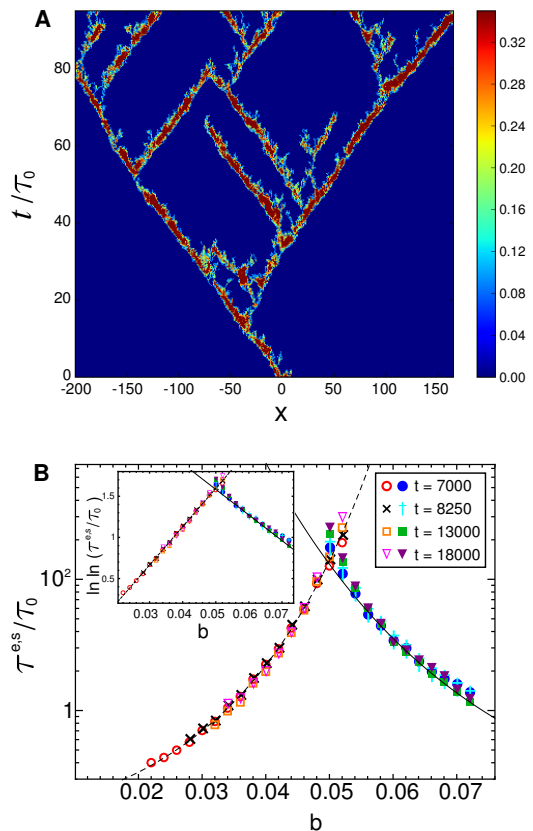


FIG. 2. Stochastic predator-prey model reproduces the phenomenology of transitional pipe turbulence. Lifetime and splitting time of clusters of prey are memoryless processes and obey super-exponential statistics as a function of prey birth rate. To compare with the experiments [8], predator-prey dynamics are performed in two-dimensional pipe geometry as described in the text. (A) World line of clusters of prey splitting to form predator-prey traveling waves. The color measures the local density of prey, corresponding to intensity of turbulence in pipe flow. In the simulation, the dimensionless parameters are $D = 0.1$, $b = 0.1$, $p = 0.2$, $d_A = 0.01$, $d_B = 0.01$ and $m = 0.001$. In the model simulated, diffusion is isotropic, not biased as would be the case corresponding to a mean flow, where the clusters will accumulate at large times with a well-defined separation set by the depletion zone of nutrient behind each predator-prey traveling wave. (B) Log lifetime of prey cluster and splitting time as a function of prey birth rate. The upward curvature signifies super-exponential behavior. The parameters are $D = 0.01$, $p = 0.1$, $d_A = 0.015$, $d_B = 0.025$ and $m = 0.001$. Inset: Double log lifetime vs prey birth rate, showing the fit to the following functional forms: the dashed curve is given by $\tau^e/\tau_0 = \exp(\exp(46.539b - 0.731))$, and the solid curve is given by $\tau^s/\tau_0 = \exp(\exp(-31.148b - 3.141))$.

into multiple clusters, as shown in the space-time plot of clusters of prey of Figure 2 (A).

To quantify these observations, we have measured both the lifetime of population clusters in the metastable region and their splitting time using a procedure directly following that of the turbulence experiments and simulations [11], and described in Appendix C. We comment

that both timescales involve implicitly measurements of quantities that exceed a given threshold, and thus it is natural that the results are found to conform to extreme value statistics [26, 28].

In Figure 2 (A) we show the phenomenology of the dynamics of initial clusters of prey, corresponding to the predator-prey analogue for the experiments in pipe flow which followed the dynamics of an initial puff of turbulence injected into the flow [8]. Depending upon the prey birth rate, the cluster decays either homogeneously or by splitting, precisely mimicking the behavior of turbulent puffs as a function of Reynolds number. The extraction from data of decay times is described in Appendix C. In Figure 2 (B) is shown the semi-log plot of lifetime for both decay and splitting as a function of prey birth rate, the upward curvature indicative of super-exponential behavior. The inset to Figure 2 (B) shows a double exponential plot of puff lifetime and splitting time vs. prey birth rate, the straight line being the fit to the functional form indicated in the caption. These figures indicate a remarkable similarity to the corresponding plots obtained for transitional pipe turbulence in both experiments [8] and direct numerical simulations [11], and demonstrate conclusively that experimental observations are well captured by an effective two-fluid model of pipe flow turbulence with predator-prey interactions between the zonal flow and the small scale turbulence.

Universality class of the laminar-turbulence transition in pipes. The two-fluid predator-prey model expressed by Equations (1) exhibits a rich phase diagram that captures the main features observed in transitional turbulence in pipes. The transition to puff-splitting can be identified with a change of stability of the spatially-uniform mean-field predator-prey coexistence point, where a stable node becomes a stable focus or spiral with increasing birth rate. In the language of predator-prey systems, this corresponds to the breakdown of spatially homogenous prey domains into periodic traveling wave states. The phase diagram is sketched in Figure 3, along with the corresponding phase diagram for transitional pipe turbulence as determined by experiment. The phenomenology of the predator-prey system mirrors that of turbulent pipe flow.

In order to determine the universality class of the non-equilibrium phase transition from laminar to turbulent flow, we use the two-fluid predator-prey mode in Equations (1). Near the transition to prey extinction, the prey population is very small and no predator can survive, and thus Equations (1) simplify to

$$\begin{aligned} B_i &\xrightarrow{d_B} E_i, & B_i + E_j &\xrightarrow[\langle ij \rangle]{b} B_i + B_j, \\ B_i + E_j &\xrightarrow[\langle ij \rangle]{D} E_i + B_j. \end{aligned} \quad (2)$$

These equations are exactly those of the reaction-diffusion model for directed percolation [35]. A more detailed and systematic way to reach this conclusion is to represent Equations 1 exactly in path integral form using

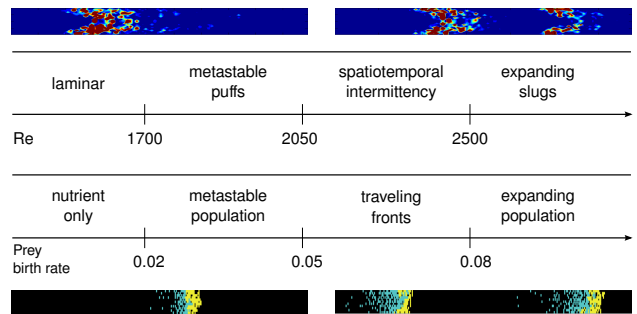


FIG. 3. Schematic phase diagram for transitional pipe turbulence as a function of Reynolds number compared with the phase diagram for predator-prey dynamics as a function of prey birth rate. Above each phase is shown a typical flow or predator-prey configuration, indicating the similarity between the turbulent pipe and ecosystem dynamics.

the Doi formalism [35–40]. The resulting action simplifies near the transition to that of Reggeon field theory [41, 42], which has been shown to be in the universality class of directed percolation [25, 43]. Numerical simulations of 3 + 1 dimensional directed percolation in a pipe geometry have reproduced the statistics and behavior of turbulent puffs and slugs in pipe flow [26, 44], and a detailed comparison between theory and experiment has been presented [45]. The super-exponential behavior of DP might seem to contradict the expectation based upon the known critical behavior (e.g., see Ref. [46]). However, it is important to recognize that the usual exponents relate to DP starting from a single seed, whereas the experiments and simulations are conducted with an extended seed that has a finite length or number of seed points. These points behave as independent identically-distributed random variables as long as the transverse correlation length is much smaller than the seed size, but once the correlation length is of order the seed size, the seed is effectively a single correlated extended source, and once the correlation length is much larger than this size, there will be a crossover to the usual DP exponents.

Discussion. The observation of the emergence of a zonal flow, excited by the developing turbulent degrees of freedom and the demonstration of its role in determining the phenomenology of transitional pipe turbulence has an interesting consequence: the zonal flow can be assisted by rotating the pipe, and this should catalyze the transition to turbulence, causing it to occur at lower Re. Indeed experiments on axially-rotating pipes [47] are consistent with this prediction.

The idea that predator-prey dynamics can arise in turbulence is by no means new, and such behavior was proposed by Diamond and collaborators [30, 48, 49] many years ago in the context of the interaction between drift-wave turbulence and zonal flows in tokomaks; indeed the predator-prey oscillations were recently observed in tokomaks [50–54] and in a table-top electroconvection analogue of the L-H transition [32]. The new ingredient we have presented in this paper is the observation of a zonal

flow emerging in the very simple setting of transitional pipe turbulence, and the demonstration of predator-prey oscillations that suggest a minimal mesoscale model of transitional turbulence that accounts for the observed statistical behavior of puffs. The observation of an emergent zonal flow and predator-prey oscillations with its attendant minimal “two-fluid” model, provide a direct and unbroken link between the Navier-Stokes equations and the directed percolation universality class for transitional turbulence. Our work underscores not only the

potential importance of zonal flows in other transitional turbulence situations, but also shows the utility of coarse-grained effective models for non-equilibrium phase transitions, even to states as perplexing as fluid turbulence.

Acknowledgements. We gratefully acknowledge helpful discussions with B. Hof, B. Eckhardt, D. Barkley, M. McIntyre, L. Kadanoff and Z. Goldenfeld. We especially thank Ashley Willis for permission to use his excellent code “Open Pipe Flow” [29]. This work was partially supported by the National Science Foundation through grant NSF-DMR-1044901.

-
- [1] O. Reynolds, *Phil. Trans. Roy. Soc. A* **174**, 935 (1883).
 [2] I. Wygnanski and F. H. Champagne, *J. Fluid Mech.* **59**, 281 (1973).
 [3] H. Faisst and B. Eckhardt, *J. Fluid Mech.* **504**, 343 (2004).
 [4] J. Peixinho and T. Mullin, *Physical Review Letters* **96**, 94501 (2006).
 [5] B. Hof, J. Westerweel, T. Schneider, and B. Eckhardt, *Nature* **443**, 59 (2006).
 [6] A. P. Willis and R. R. Kerswell, *Phys. Rev. Lett.* **98**, 014501 (2007).
 [7] B. Song and B. Hof, *Journal of Statistical Mechanics: Theory and Experiment* **2014**, P02001 (2014).
 [8] B. Hof, A. de Lozar, D. J. Kuik, and J. Westerweel, *Phys. Rev. Lett.* **101**, 214501 (2008).
 [9] I. Wygnanski, M. Sokolov, and D. Friedman, *J. Fluid Mech.* **59**, 283 (1975).
 [10] D. Moxey and D. Barkley, *Proc. Natl. Acad. Sci. USA* **107**, 8091 (2010).
 [11] K. Avila, D. Moxey, A. de Lozar, M. Avila, D. Barkley, and B. Hof, *Science* **333**, 192 (2011).
 [12] M. Nishi, Bülent Ünsal, F. Durst, and G. Biswas, *J. Fluid Mech.* **614**, 425 (2008).
 [13] G. Lemoult, K. Gumowski, J.-L. Aider, and J. E. Wesfreid, *The European Physical Journal E* **37**, 1 (2014).
 [14] D. Borrero-Echeverry, M. F. Schatz, and R. Tagg, *Phys. Rev. E* **81**, 025301 (2010).
 [15] A. P. Willis, P. Cvitanović, and M. Avila, *Journal of Fluid Mechanics* **721**, 514 (2013).
 [16] P. Cvitanović, *Journal of Fluid Mechanics* **726**, 1 (2013).
 [17] R. Kerswell, *Nonlinearity* **18**, R17 (2005).
 [18] B. Eckhardt, T. M. Schneider, B. Hof, and J. Westerweel, *Annual Review of Fluid Mechanics* **39**, 447 (2007).
 [19] G. Kawahara, M. Uhlmann, and L. van Veen, *Annual Review of Fluid Mechanics* **44**, 203 (2012).
 [20] M. Avila, F. Mellibovsky, N. Roland, and B. Hof, *Physical Review Letters* **110**, 224502 (2013).
 [21] M. Chantry, A. P. Willis, and R. R. Kerswell, *Physical Review Letters* **112**, 164501 (2014).
 [22] J. P. Crutchfield and K. Kaneko, *Physical Review Letters* **60**, 2715 (1988).
 [23] D. Barkley, *Physical Review E* **84**, 016309 (2011).
 [24] Y. Pomeau, *Physica* **23D**, 3 (1986).
 [25] H. Janssen, *Zeitschrift für Physik B Condensed Matter* **42**, 151 (1981).
 [26] M. Sipos and N. Goldenfeld, *Physical Review E* **84**, 035304 (2011).
 [27] J. Peixinho and T. Mullin, *Journal of Fluid Mechanics* **582**, 169 (2007).
 [28] N. Goldenfeld, N. Guttenberg, and G. Gioia, *Phys. Rev. E* **81**, 035304 (2010).
 [29] A. P. Willis and R. R. Kerswell, *J. Fluid Mech.* **619**, 213 (2009).
 [30] P. H. Diamond, Y.-M. Liang, B. A. Carreras, and P. W. Terry, *Phys. Rev. Lett.* **72**, 2565 (1994).
 [31] G. Sivashinsky and V. Yakhot, *Physics of Fluids (1958-1988)* **28**, 1040 (1985).
 [32] L. Bardóczy, A. Bencze, M. Berta, and L. Schmitz, *Physical Review E* **90**, 063103 (2014).
 [33] J. B. Parker and J. A. Krommes, *New Journal of Physics* **16**, 035006 (2014).
 [34] N. Goldenfeld, *Lectures On Phase Transitions And The Renormalization Group* (Addison-Wesley Reading, MA, 1992).
 [35] G. Ódor, *Reviews of Modern Physics* **76**, 663 (2004).
 [36] M. Doi, *Journal of Physics A: Mathematical and General* **9**, 1465 (1976).
 [37] P. Grassberger and M. Scheunert, *Fortschritte der Physik* **28**, 547 (1980).
 [38] A. Mikhailov, *Physics Letters A* **85**, 214 (1981).
 [39] N. Goldenfeld, *Journal of Physics A Mathematical General* **17**, 2807 (1984).
 [40] D. C. Mattis and M. L. Glasser, *Reviews of Modern Physics* **70**, 979 (1998).
 [41] M. Mobilia, I. T. Georgiev, and U. C. Täuber, *Journal of Statistical Physics* **128**, 447 (2007).
 [42] U. C. Täuber, *Journal of Physics A: Mathematical and Theoretical* **45**, 405002 (2012).
 [43] J. L. Cardy and R. L. Sugar, *Journal of Physics A: Mathematical and General* **13**, L423 (1980).
 [44] K. T. Allhoff and B. Eckhardt, *Fluid Dynamics Research* **44**, 031201 (2012).
 [45] L. Shi, M. Avila, and B. Hof, *arXiv preprint arXiv:1504.03304* (2015).
 [46] H. H. Hinrichsen, *Advances in Physics* **49**, 815 (2000).
 [47] M. Murakami and K. Kikuyama, *Journal of Fluids Engineering* **102**, 97 (1980).
 [48] E.-j. Kim and P. H. Diamond, *Phys. Rev. Lett.* **90**, 185006 (4 pages) (2003).
 [49] K. Itoh, S.-I. Itoh, P. H. Diamond, T. S. Hahm, A. Fujisawa, G. R. Tynan, M. Yagi, and Y. Nagashima, *Physics of Plasmas* **13**, 055502 (2006).
 [50] T. Estrada, T. Happel, C. Hidalgo, E. Ascasbar, and E. Blanco, *EPL* **92**, 35001 (6 pages) (2010).

- [51] G. D. Conway, C. Angioni, F. Ryter, P. Sauter, and J. Vicente (ASDEX Upgrade Team), *Phys. Rev. Lett.* **106**, 065001 (4 pages) (2011).
- [52] G. S. Xu, B. N. Wan, H. Q. Wang, H. Y. Guo, H. L. Zhao, A. D. Liu, V. Naulin, P. H. Diamond, G. R. Tynan, M. Xu, R. Chen, M. Jiang, P. Liu, N. Yan, W. Zhang, L. Wang, S. C. Liu, and S. Y. Ding, *Phys. Rev. Lett.* **107**, 125001 (5 pages) (2011).
- [53] T. Estrada, C. Hidalgo, T. Happel, and P. H. Diamond, *Phys. Rev. Lett.* **107**, 245004 (5 pages) (2011).
- [54] L. Schmitz, L. Zeng, T. L. Rhodes, J. C. Hillesheim, E. J. Doyle, R. J. Groebner, W. A. Peebles, K. H. Burrell, and G. Wang, *Phys. Rev. Lett.* **108**, 155002 (5 pages) (2012).
- [55] A. J. Lotka, *The Journal of Physical Chemistry* **14**, 271 (1910).
- [56] V. Volterra, *Variazioni e fluttuazioni del numero d'individui in specie animali conviventi* (C. Ferrari, 1927).
- [57] E. Renshaw, *Modelling biological populations in space and time*, Vol. 11 (Cambridge University Press, 1993).
- [58] A. J. McKane and T. J. Newman, *Physical Review Letters* **94**, 218102 (2005).

SUPPLEMENTARY MATERIAL

Appendix A: Direct numerical simulations of the Navier-Stokes equations.

We performed direct numerical simulations (DNS) of the Navier-Stokes equations in a pipe, using the open-source code “Open Pipe Flow” [29]. The equations were solved using a pseudo-spectral method in cylindrical coordinates [29], having 60 grid points in the radial (r) direction, 32 Fourier modes in the azimuthal (θ) direction and 128 modes in the axial (z) direction. Such a model is of course a reduced description of reality, but the main features can be well captured, with a slight renormalization of the Re needed to compare with experiment [29]. For the accuracy required in our study, we used 32 modes in the azimuthal direction, compared to only 2 used by Willis and Kerswell [29]. The spatial resolutions were chosen such that the resolvable power spectra span over six orders of magnitude. The pipe length L is 20 times its radius R , with periodic boundary conditions in the z direction [29]. With this resolution, the transition to turbulence occurs in a range of Re numbers between 2200 and 3000, and moves to smaller Re at still higher resolution. We report here measurements at $\text{Re} = 2600$, slightly above the transition [11]. The mass flux and $\text{Re} = 2600$ were held constant in time [29]. The laminar flow is the Hagen–Poiseuille flow, which was independent of time as the mass flux was held constant [29].

Appendix B: Stochastic simulations of predator-prey dynamics.

The specific system has three trophic levels: nutrient (E), Prey (B) and Predator (A), which correspond in

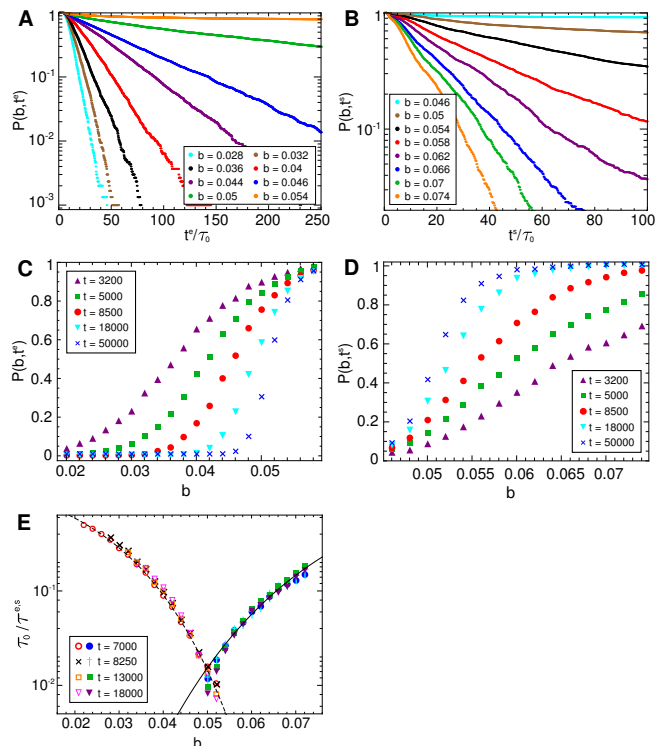


FIG. S1. Stochastic predator-prey model reproduces the phenomenology of transitional pipe turbulence. Lifetime and splitting time of clusters of prey are memoryless processes and obey super-exponential statistics as a function of prey birth rate. To compare with the experiments [8], predator-prey dynamics are performed in two-dimensional pipe geometry as described in the text. The dimensionless parameters in the simulation are $D = 0.01$, $p = 0.1$, $d_A = 0.015$, $d_B = 0.025$ and $m = 0.001$. (A) Log survival probability of prey cluster vs. time during homogeneous decay to extinction. Here the characteristic time scale that is estimated by $\tau_0 \sim 200$. (B) Log survival probability of prey cluster vs. time during decay to splitting. (C) Survival probability of prey cluster as a function of prey birth rate during homogeneous decay to extinction. (D) Survival probability of prey cluster as a function of prey birth rate during decay to splitting. (E) Log inverse lifetime of prey cluster, as a function of prey birth rate during homogeneous decay to extinction (left curve, τ^e) and during decay to splitting (right curve, τ^s). The dashed curve is given by $\tau_0/\tau^e = 1/\exp(\exp(46.539b - 0.731))$, and the solid curve is given by $\tau_0/\tau^s = 1/\exp(\exp(-31.148b - 3.141))$.

the fluid system to laminar flow, turbulence and zonal flow respectively. Such a system can be naively modeled by the Lotka-Volterra ordinary differential equations [55–57], which in the case of ecosystems with finite resources do not permit long-time persistent oscillatory solutions, unless additional biological details such as functional response are included. In fact, it is necessary to include the dynamics of individual birth-death events, and when this is done correctly, it is found that the number fluctuations drive the population oscillations [58] through resonant amplification. Thus, we use a stochastic model at the outset.

The interactions between individual representatives of these levels are given by Equations 1. We simulated these equations on a 401×11 lattice in two dimensions, intended to emulate the pipe geometry. Lattice sites were only allowed to be occupied by one of E, A or B. The predator (A) and prey (B) are additionally allowed to diffuse via random walk on the lattice with diffusion coefficient 0.1 in units of the square of the lattice spacing divided by the time step (set equal to unity). The initial conditions for the simulations were a random population of prey and predator, occupying with probability $4/5$ and $1/5$ respectively on the lattice sites between $x \in [-15, 15]$ and $y \in [-5, 5]$ where x labels the direction along the axis of the ecosystem (pipe) and y labels the transverse direction. The predator-prey dynamics in Eq. 1 was implemented by the following algorithm: at each time step, a site i is randomly chosen, a random number s , is generated from the uniform distribution between zero and one. The behavior on the site is decided by the random number: (1) if $s < 1/6$ and the site i is occupied by any individual, and if a randomly chosen neighbor site is empty, then that individual diffuses to the random neighboring site with rate $\mu = 0.01$ (i.e. this reaction happens if another uniformly distributed random number is less than $1 - \exp \mu$); (2) if $1/6 \leq s < 1/3$ and the site i is occupied by a prey individual, and if a randomly chosen neighbor site, j , is empty, then one prey individual is born on the site j with rate b ; (3) if $1/3 \leq s < 1/2$ and the site i is occupied by a predator individual, and if a randomly chosen neighbor site, j , is occupied by a prey individual, then the prey individual is replaced by a new-born predator individual with rate p ; (4) if $1/2 \leq s < 2/3$ and the site i is occupied by a predator individual, that predator individual dies with rate d_A ; (5) if $2/3 \leq s < 5/6$ and the site i is occupied by a prey individual, that prey individual dies with rate d_B ; (6) if $5/6 \leq s < 1$ and the site i is occupied by a prey individual, then the prey individual is replaced by a predator individual with rate m . Then within the same time step, the above processes are repeated 401×11 times so that on average one reaction takes place at each lattice site in the system.

Appendix C: Measurement of decay and splitting lifetimes.

We measured both the lifetime of population clusters in the metastable region and their splitting time using a procedure directly following that of the turbulence experiments and simulations [11]. To this end, we monitor the coarse-grained prey population density $\tilde{n}_B(i) = \sum_{j=-J}^{j=J} \sum_{l=-H/2}^{l=H/2} n_B(i+j, l) / (H+1)/(2J+1) - 0.25$, where H is the height of the system (11 lattice units) and $J = 3$. The lifetime of prey clusters is defined as the time it takes for the last prey individual to die. The cluster splitting time is defined as the first time that the distance between the edges of two coarse-grained prey clusters exceed 25 unit sites. We comment that both timescales involve implicitly measurements of quantities that exceed a given threshold, and thus it is natural that the results are found to conform to extreme value statistics [26, 28].

In Figure S1 we show the phenomenology of the dynamics of initial clusters of prey, corresponding to the predator-prey analogue for the experiments in pipe flow which followed the dynamics of an initial puff of turbulence injected into the flow [8]. Depending upon the prey birth rate, the cluster decays either homogeneously or by splitting, precisely mimicking the behavior of turbulent puffs as a function of Reynolds number. Figure S1 (A) and (B) show that the decay is exponential in time, indicating that it is a memoryless process with a single time constant. Figure S1 (C) and (D) show that the survival probability is a sigmoidal curve, whose inverse lifetime as a function of prey birth rate is plotted in a log-linear scale in Figures S1 (E) and (F). If the lifetime were an exponential function, this curve would be a straight line with negative slope. The downward curvature is a manifestation of super-exponential behavior. These figures indicate a remarkable similarity to the corresponding plots obtained for transitional pipe turbulence in both experiments [8] and direct numerical simulations [11], and demonstrate conclusively that experimental observations are well captured by an effective two-fluid model of pipe flow turbulence with predator-prey interactions between the zonal flow and the small scale turbulence.